

# Endocortical bone loss in osteoporosis: the role of bone surface availability

Pascal R Buenzli<sup>a,1</sup>, C David L Thomas<sup>b</sup>, John G Clement<sup>b</sup>, Peter Pivonka<sup>a</sup>

<sup>a</sup>Faculty of Engineering, Computing & Mathematics, The University of Western Australia, WA 6009, Australia

<sup>b</sup>School of Dental Science, University of Melbourne, VIC 3010, Australia

October 16, 2019

**Abstract** – Age-related bone loss and postmenopausal osteoporosis are disorders of bone remodelling, in which less bone is reformed than resorbed. Yet, this dysregulation of bone remodelling does not occur equally in all bone regions. Loss of bone is more pronounced near the endocortex, leading to cortical wall thinning and medullary cavity expansion, a process sometimes referred to as “trabecularisation” or “cancellisation”. Cortical wall thinning is of primary concern in osteoporosis due to the strong reduction in bone mechanical properties that it is associated with. In this paper, we examine the possibility that the nonuniformity of microscopic bone surface availability could explain the nonuniformity of bone loss in osteoporosis. We use a simple computational model of bone remodelling, in which microscopic bone surface availability influences bone turnover rate, to simulate the evolution of the bone volume fraction profile across the midshaft of a long bone. We find that bone loss is accelerated near the endocortical wall where the specific surface is highest. Over time, this leads to a substantial reduction of cortical wall width from the endosteum. The associated expansion of the medullary cavity can be made to match experimentally observed data from cross-sectional studies in the Melbourne Femur Collection. Finally, we calculate the redistribution of the stresses in this evolving bone structure and show that mechanical load becomes critically transferred on periosteal cortical bone.

**Key words:** osteoporosis, cortical wall thinning, medullary cavity expansion, bone remodelling, specific surface, mathematical modelling

## 1 Introduction

It is well known that cortical porosity of bone increases in osteoporosis leading to a reduction in bone stiffness and strength, ultimately increasing the risk of fracture [1–7]. The temporal evolution of this deterioration in single individuals is still poorly understood. Most of our current knowledge is deduced from cross-sectional data collected by micro-computed tomography of bones. These data indicates that changes in cortical porosity are not uniformly distributed across the cortical thickness. In particular, in long bones, loss is more pronounced near the endocortical surface [1–4, 8]. Age-related bone loss is therefore characterized by an expansion of the marrow (or medullary) cavity. This process is often referred to as “trabecularisation” of cortical bone, since the aged cortical bone exhibits morphological similarities with trabecular bone [8]. In the following, we refer to this nonuniform bone loss of cortical bone as *endocortical bone loss*. Endocortical bone loss results in a reduction

in cortical wall thickness and in an increase in porosity which consequently reduces the load-bearing capacity of bone.

Several mechanisms have been hypothesised to drive bone loss in osteoporosis, including hormonal changes, reduced physical activity, and an evolving bone micro-structure leading to changes in bone surface availability. Hormonal changes are associated with increased remodelling activity, reduction in osteoblast activity, reduction in osteoblast number, and bone imbalance per basic multicellular unit (BMU) [4, 9, 10]. To explain the nonuniformity of age-related bone loss, RB Martin suggested that bone loss may be influenced by the microscopic availability of bone surface [11, 12]. In fact, based on experimental data, Martin exhibited a remarkable relationship between bone porosity and bone specific surface (i.e., surface area per volume of bone tissue). Using this relationship, Martin found from a simple mathematical model that in cortical bone increased resorption activity of bone cells would lead to an increase in surface area which in turn would lead to a further increase in resorption activity, hence, creating a morphological

<sup>1</sup>Corresponding author. Email address:  
pascal.buenzli@uwa.edu.au

(or geometrical) feedback [11]. In trabecular bone this situation is reversed. Martin’s hypothesis that bone remodelling in osteoporosis contains such a morphological feedback by the evolving bone micro-structure is difficult to study experimentally and Martin did not provide any comparison to experimental data. Indeed, the time scales involved in osteoporosis are large, and there is no easy experimental control of the strength of the morphological feedback, nor of how bone morphology changes with age.

In this paper we propose a computational modelling approach suited to the investigation of the nonuniformity of bone loss in osteoporosis as due to a morphological regulation. Changes in cortical bone volume fraction occurring in the midshaft of human femur bone are evolved numerically assuming an initial bone state and an osteoporotic condition. Our computational model follows Martin’s idea [11, 12]: we hypothesise that the experimentally observed nonuniform deterioration of bone in osteoporosis is due to the superposition of:

- (i) Hormonal changes and/or changes in the overall loading, leading to a uniform baseline of bone loss across the cortical bone;
- (ii) An evolving bone micro-structure, that locally increases or decreases bone remodelling activity (by morphological feedback), and so locally increases or decreases bone loss compared to the hormonal/mechanical baseline.

We then hypothesise that the above mechanisms are able to explain (at least in part) the rate of endocortical bone loss that the expansion of the medullary cavity represents, for which there is experimental data available [2]. The predominant loss of bone in the endocortical region is expected to increasingly transfer mechanical loading towards the periosteum.

To test these hypotheses we extend the (purely temporal) mathematical model initially proposed by Martin [12] to include a spatial component. This spatio-temporal description enables us to follow the evolution of the distribution of bone volume fraction across the midshaft of a long bone. The feedback of bone morphology on the bone cells is implemented using the phenomenological relationship between bone specific surface and bone porosity mentioned above. Furthermore, we investigate changes in the mechanical stress distribution across the midshaft due to this evolving bone microstructure. The distribution of the stresses are calculated using an extension of classical beam theory to materials of nonuniform composition. This theory and the mathematical model of bone

remodelling are presented in Section 2. The numerical results are shown in Section 3 and discussed in Section 4.

## 2 Methods

In this section, we first present a simple mathematical model of bone remodelling well-suited to investigate the role of nonuniform bone surface availability for endocortical bone loss in osteoporosis. We then present the method by which the redistribution of the internal stresses will be calculated when bone has evolving nonuniform internal properties.

### Computational model of bone remodelling including morphological regulation

Bone remodelling is a complex metabolic process that involves regulations at several time scales and length scales. To follow the evolution of bone properties that are relevant to the macroscopic degradation of bone in osteoporosis, we consider a computational model focused on a millimetre-size tissue scale. This observation scale is large enough for local resorption and formation processes to be of macroscopic significance for the mechanical and microstructural properties of the tissue [13, 14] and small enough for the cellular origin of resorption and formation to be considered with biochemical and morphological regulations [15, 16]. At the tissue scale, the various cell populations involved in bone remodelling can be represented by continuous variables, i.e. local cell densities  $n(\mathbf{r}, t)$ , by means of local averages over a so-called ‘representative volume element’ (RVE) of the tissue  $V_T \approx 3\text{--}8 \text{ mm}^3$ :

$$n(\mathbf{r}, t) \equiv \frac{N(\mathbf{r}, t)}{V_T}, \quad (1)$$

where  $N(\mathbf{r}, t)$  is the number of cells in the volume  $V_T$  centred at position  $\mathbf{r}$ , at time  $t$  (Figure 1a).

Stiffness properties of a millimetre-size portion of bone tissue are determined to a great extent by the bone volume fraction (or equivalently the bone porosity) and the elastic properties of the mineralised bone matrix [13].<sup>1</sup> In osteoporosis, both bone volume fraction and the degree of mineralisation of bone matrix are decreased. Osteoporosis is associated with increased remodelling activity with net bone loss per

<sup>1</sup>Generally speaking, pore shape is another important factor determining stiffness properties of porous materials. In cortical bone, however, pores are fairly uniformly cylindrical (Haversian canals) and their distribution within cross-sections, for example, is unimportant for tissue stiffness at the millimetre-scale [14].

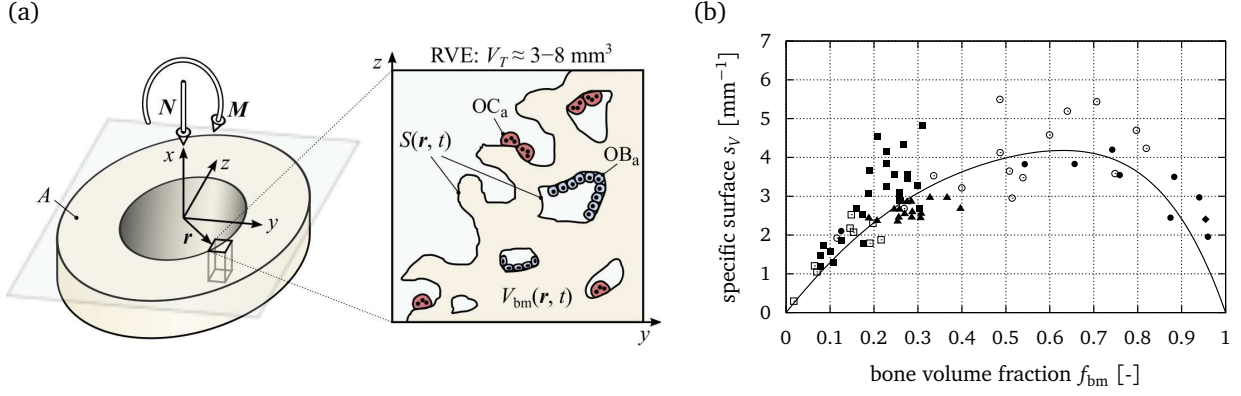


**Figure 1** – (a) Compressive force  $N$  and bending moment  $M$  acting in a cross-section (of area  $A$ ) of a long bone. The representative volume element (RVE) of the tissue at position  $\mathbf{r}$  serves to define local spatial averages of bone properties, such as cell densities, bone matrix volume fraction  $f_{bm}$  and specific surface  $s_V$ . (b) Relationship between specific surface  $s_V$  and bone matrix volume fraction  $f_{bm}$  as in Eq. (7). (Redrawn from Ref. [12])

remodelling event that evolves stronger with time [4]. This rapid remodelling both exacerbates bone loss and replaces more densely mineralised matrix with younger, undermineralised matrix [17]. In this paper, we focus on age-related changes in the morphological rather than mineral properties of the bone tissue. Such morphological changes have been extensively studied in cadaver bone specimens from the Melbourne Femur Collection [2]. Changes in the degree of mineralisation of bone matrix will be studied in future works. The bone volume fraction  $f_{bm}(\mathbf{r}, t)$  of a portion of bone tissue represents the amount of bone matrix (volume  $V_{bm}$ ) in the RVE:<sup>2</sup>

$$f_{bm}(\mathbf{r}, t) \equiv \frac{V_{bm}(\mathbf{r}, t)}{V_T}. \quad (2)$$

Local bone matrix is continually renewed by remodelling. In homeostasis, resorption and formation are balanced and remodelling leads to bone turnover without loss or gain.<sup>3</sup> In osteoporosis, less bone is reformed than resorbed, so bone turnover is associated with a net bone loss. The evolution of the local bone volume fraction  $f_{bm}$  is governed by (i) the local densities of active osteoblasts ( $OB_a$ ) and active

osteoclasts ( $OC_a$ ) and (ii) these cells' activity rates:

$$\frac{\partial}{\partial t} f_{bm}(\mathbf{r}, t) = k_{form} OB_a(\mathbf{r}, t) - k_{res} OC_a(\mathbf{r}, t), \quad (3)$$

where  $k_{form}$  is the volume of new bone synthesised per unit time by a single active osteoblast and  $k_{res}$  the volume of bone resorbed per unit time by a single active osteoclast.

Equation (3) holds very generally. It expresses the balance between bone formation and bone resorption:  $k_{form} OB_a$  corresponds to the formation rate (bone volume fraction synthesised per unit time) whilst  $k_{res} OC_a$  corresponds to the resorption rate (bone volume fraction resorbed per unit time). The difficulty in Eq. (3) lies in determining the evolution of the densities of active osteoclasts and active osteoblasts, and in particular, in determining how these densities depend themselves on the presence of bone matrix. Indeed, osteoclasts and osteoblasts require a pre-existing bone substrate to conduct their resorbing and synthesising activities. The densities of osteoclasts and osteoblasts thus depend on the local amount of bone surface (area  $S$ ) available to them in the RVE, i.e., on the specific surface  $s_V(\mathbf{r}, t)$ :<sup>4</sup>

$$s_V(\mathbf{r}, t) \equiv \frac{S(\mathbf{r}, t)}{V_T}. \quad (4)$$

Comprehensive cell population models of osteoblasts and osteoclasts including biochemical coupling have been proposed in the literature [15, 21, 22]. In Ref. [23], the potential influence of the specific surface on various stages of osteoblast and osteoclast developments was investigated in the bone cell population model [15]. Here, however, we will consider a simpler model of bone cells, originally

<sup>2</sup>The bone volume fraction  $f_{bm}$  is also equal to  $1 - \Phi$ , where  $\Phi$  is the bone porosity. In Ref. [15],  $f_{bm}$  was denoted by  $bv$ .

<sup>3</sup>In cortical bone, remodelling generates both type I osteons, associated with a new Haversian canal, and type II osteons, associated with a pre-existing Haversian canal [18, 19]. The creation of a new Haversian canal in type I osteons therefore always implies a net bone loss [20]. However, the exact proportion of type I over type II osteons in normal remodelling remains controversial. Whilst the density of vascular channels was shown to increase progressively with age [19], age-related bone loss was shown to be associated with an increase in pore area rather than an increase in pore density [7]. The importance of cortical bone loss with age due to normal remodelling is thus difficult to estimate. In the present model, we do not take this effect into account and assume the same baseline of bone imbalance per remodelling event in trabecular and cortical bone for simplicity.

<sup>4</sup>We do not include surfaces of the canalicular system in this definition of  $s_V$ . Canalicular surfaces are not available to osteoclasts and osteoblasts for remodelling.

formulated by Martin [12], in which the dependence of active osteoclasts and active osteoblasts upon  $s_V$  appears explicitly. This model is already able to illustrate how a nonuniform distribution of specific surface across a bone midshaft may influence age-related bone degradation differently in different regions of the tissue, and how this may lead to rates of endocortical bone loss with associated cortical wall thinning and medullary cavity expansion matching experimental data.

Bone tissues with a large specific surface exhibit more remodelling, and so have more active osteoblasts and active osteoclasts, than tissues with a small specific surface (Figure 1a). Denoting by  $\lambda_{OB_a}$  and  $\lambda_{OC_a}$  the fractions of the bone surface at which there is osteoblastic and osteoclastic activity due to remodelling, and by  $\sigma_{OB_a}$  and  $\sigma_{OC_a}$  the surface densities of active osteoblasts and active osteoclasts at these sites, the densities of active osteoblasts and active osteoclasts are given by  $OB_a = \lambda_{OB_a} \sigma_{OB_a} s_V$  and  $OC_a = \lambda_{OC_a} \sigma_{OC_a} s_V$ . Substituting these expressions in Eq. (3), one thus has [12]:

$$\frac{\partial}{\partial t} f_{bm}(\mathbf{r}, t) = (k_{form} \lambda_{OB_a} \sigma_{OB_a} - k_{res} \lambda_{OC_a} \sigma_{OC_a}) s_V(\mathbf{r}, t). \quad (5)$$

Whilst Eq. (5) holds again in full generality, in the following, it is assumed that  $k_{form}$ ,  $k_{res}$ ,  $\lambda_{OB_a}$ ,  $\lambda_{OC_a}$ ,  $\sigma_{OB_a}$ ,  $\sigma_{OC_a}$  can be taken uniform and constant in time. This is clearly a simplification, as the microscopic availability of bone surface may in principle influence the recruitment and development of bone cells in a nontrivial way. These recruitment and development processes determine the fractions  $\lambda_{OB_a}$  and  $\lambda_{OC_a}$ , which would thus normally be expected to depend additionally on  $s_V$ . Here, a simple extensivity in  $s_V$  is assumed when taking  $OB_a$  and  $OC_a$  just proportional to  $s_V$ .

In osteoporosis, a net bone loss is associated to each remodelling event. To retrieve physiological overall rates of bone loss, Martin assumed a small imbalance between formation and resorption, setting:

$$k_{form} \lambda_{OB_a} \sigma_{OB_a} - k_{res} \lambda_{OC_a} \sigma_{OC_a} = -2 \mu\text{m/year}. \quad (6)$$

This constant baseline of bone loss means that a 2  $\mu\text{m}$ -thick layer of bone matrix is resorbed each year on all bone surfaces. This baseline of bone loss is weighted by the specific surface to correspond to volumetric losses.

Bone tissues exhibit a wide range of microstructures, each characterising a particular volume fraction and specific surface. Cortical bone typically has volume fractions  $f_{bm} \approx 0.85\text{--}0.95$  with pores mainly constituted of Haversian canals. Trabecular bone

typically has volume fractions  $f_{bm} \approx 0.15\text{--}0.55$  with ‘pores’ corresponding to the marrow space around the trabecular plates and struts. Based on measurements performed in a large variety of bone tissues, Martin [12] has proposed that bone volume fraction  $f_{bm}$  and specific surface  $s_V$  follow an ‘intrinsic’ or ‘universal’ relationship, approximated by the following polynomial:

$$s_V(f_{bm}) = a_1 f_{bm} + a_2 f_{bm}^2 + a_3 f_{bm}^3 + a_4 f_{bm}^4 + a_5 f_{bm}^5, \quad (7)$$

with

$$a_1 = 14.1/\text{mm}, \quad a_2 = -10.5/\text{mm}, \quad a_3 = -17.8/\text{mm}, \\ a_4 = 43.0/\text{mm}, \quad a_5 = -28.8/\text{mm}. \quad (8)$$

The relation (7) is plotted in Figure 1b together with experimental data assembled in Ref. [12] from various types of human bones (femur, iliac crest, vertebra, rib) both in health and disease.<sup>5</sup> Importantly, the specific surface exhibits a maximum  $s_V^* \approx 4.2/\text{mm}$  at a bone volume fraction  $f_{bm}^* \approx 0.63$ , intermediate between cortical and trabecular bone.

Using the phenomenological relation (7) in Eq. (5), one is able to calculate the evolution of bone volume fraction  $f_{bm}(\mathbf{r}, t)$  in every region  $\mathbf{r}$  of the bone tissue, given an initial distribution of volume fraction  $f_{bm}(\mathbf{r}, 0)$ . This evolution enables us to determine how the medullary cavity expands in time for comparison with experimental data [2]. It is well-known that the distinction between cortical and trabecular bone is not straightforward in osteoporosis [8]. Similarly, measuring the extent of the medullary cavity relies on a visual threshold. For the purpose of this paper, we assume that the medullary cavity is defined by the region of bone tissue in which bone volume fraction is lower than a threshold  $f_{bm}^*$ . We will take this threshold as the volume fraction at which the specific surface is maximum according to Eq. (7), i.e.  $f_{bm}^* \approx 0.63$ . The effect of choosing different threshold values for the determination of medullary cavity radius is shown in Figure 2d.

The simplicity of the model considered here has two practical consequences: (i) the specific surface  $s_V$  enters as an explicit dependence in the right hand side of Eq. (5). This allows to find a semi-analytical solution of the evolution of bone volume fraction  $f_{bm}$  (see Appendix A); (ii) the current state of the bone tissue system only depends on the current distribution profile of the bone volume fraction. This enables

<sup>5</sup>This figure is redrawn from Ref. [12] with the bone volume fraction  $f_{bm}$  in lieu of the porosity  $1 - f_{bm}$ . The coefficients  $a_1, \dots, a_5$  of the phenomenological polynomial have been slightly adjusted from [12] such that  $s_V(0) = s_V(1) = 0$ .



us to easily evolve the system backwards in time and to determine the volume fraction profile in the endocortical region that results in a given medullary cavity expansion (see Appendix B).

### Internal stress distribution

Mechanical loading is carried nonuniformly by bone tissues. In particular, the cortex carries much of the loads applied to a bone [8]. To estimate how internal mechanical stresses are redistributing across the midshaft section of a long bone during age-related degradation of the endocortex, we use a simple theory of elasticity for beams of nonuniform composition (see [24–26] and Refs cited therein). This theory is based on two main assumptions:

1. Hooke's law is valid locally at the tissue scale, i.e., the stress tensor field  $\sigma(\mathbf{r}, t)$  and strain tensor field  $\varepsilon(\mathbf{r}, t)$  are related by a local stiffness  $E(\mathbf{r}, t)$  of the tissue:

$$\sigma(\mathbf{r}, t) = E(\mathbf{r}, t)\varepsilon(\mathbf{r}, t) \quad (9)$$

2. Near the midshaft of a long bone, small deformations generated by compression and bending keep the initial cross-sections planar and normal to the neutral axis. This geometrical constraint on the deformations is called the Euler–Bernoulli condition.

From a structural point of view, long bones near the midshaft can be regarded as weakly-deformed long beams, for which the Euler–Bernoulli condition is well approximated. At small deformations, only strains in the longitudinal  $x$  axis of the bone need to be considered, i.e.,  $\varepsilon(\mathbf{r}, t)$  reduces to the single scalar component  $\varepsilon_{xx}(\mathbf{r}, t)$ . Similarly, shear strains are neglected and the strain tensor is assumed to reduce to the single component  $\sigma_{xx}(\mathbf{r}, t)$  [27, §17]. Therefore, only a single component of the stiffness tensor field needs to be considered in Eq. (9). Later, this stiffness field will be assumed to be a function of bone volume fraction only, i.e.,  $E(\mathbf{r}, t) = E(f_{\text{bm}}(\mathbf{r}, t))$ .

In the following, we therefore focus on a long bone cross-section performed at a level  $x$  located near the midshaft. We use the position vector  $\mathbf{y} = (y, z)$  to denote a position in the cross-sectional plane and omit both the cross-section level  $x$  and the component indices  $xx$  from the notation. We assume that this bone is subject to a compressive resultant force  $N(t) = -N(t)\mathbf{e}_x$  along  $x$  and a resultant bending moment  $\mathbf{M}(t) = M_y(t)\mathbf{e}_y + M_z(t)\mathbf{e}_z$  in the cross-sectional  $\mathbf{y}$  plane (see Figure 1a). By definition, these resultant force and moment are given as integrals of

the strain field  $\sigma(\mathbf{r}, t)$ . With Hooke's law (9), one thus has:

$$N(t) = \int_A d\mathbf{y} E(\mathbf{y}, t) \varepsilon(\mathbf{y}, t), \quad (10)$$

$$M_y(t) = - \int_A d\mathbf{y} z E(\mathbf{y}, t) \varepsilon(\mathbf{y}, t), \quad (11)$$

$$M_z(t) = \int_A d\mathbf{y} y E(\mathbf{y}, t) \varepsilon(\mathbf{y}, t), \quad (12)$$

where the integrals are carried over the bone cross-sectional area  $A$ . The geometric constraint imposed by the Euler–Bernoulli condition requires the strain field  $\varepsilon(\mathbf{y}, t)$  to be a linear function of the transverse spatial coordinates  $\mathbf{y} = (y, z)$  (see Figure (1)a):

$$\varepsilon(\mathbf{y}, t) \equiv \varepsilon_0(t) + \varepsilon_y(t)y + \varepsilon_z(t)z \quad (13)$$

At each time  $t$ , the Euler–Bernoulli condition (13) together with the constraints (10)–(12) form a system of three linear equations determining the three unknown  $\varepsilon_0(t)$ ,  $\varepsilon_y(t)$  and  $\varepsilon_z(t)$ . The coefficients of this system of equations involve zero order, first order and second order inertial moments of the material weighted by the nonuniform stiffness, i.e.:

$$\begin{aligned} I_0(t) &\equiv \int_A d\mathbf{y} E(\mathbf{y}, t), & I_j(t) &\equiv \int_A d\mathbf{y} x_j E(\mathbf{y}, t), \\ I_{jk} &\equiv \int_A d\mathbf{y} x_j x_k E(\mathbf{y}, t), & i, j &= 2, 3 \end{aligned} \quad (14)$$

(with  $x_2 = y$  and  $x_3 = z$ ). Once  $\varepsilon_0(t)$ ,  $\varepsilon_y(t)$  and  $\varepsilon_z(t)$  are known, the stress field distribution in the cross-section is then given by use of Hooke's law:

$$\sigma(\mathbf{y}, t) = E(\mathbf{y}, t) [\varepsilon_0(t) + \varepsilon_y(t)y + \varepsilon_z(t)z] \quad (15)$$

The inertial moments (14) determining the coefficients of the system of equations to solve are specified by assuming a simple nonlinear phenomenological relationship between stiffness and bone volume fraction [28]:

$$E(\mathbf{y}, t) = C f_{\text{bm}}(\mathbf{y}, t)^3, \quad (16)$$

where  $C \approx 15$  GPa and  $f_{\text{bm}}(\mathbf{y}, t)$  is governed by the balance equation (5).

## 3 Results

Equation (5) determines the evolution of the bone volume fraction  $f_{\text{bm}}(\mathbf{r}, t)$  at each position  $\mathbf{r}$  within bone from a given initial condition  $f_{\text{bm}}(\mathbf{r}, t=0)$ . Here

for simplicity only rotation-symmetric initial distributions are considered, implying that  $f_{\text{bm}}$  stays rotation-symmetric at all times:  $f_{\text{bm}}(\mathbf{r}, t) = f_{\text{bm}}(y, z, t) = f_{\text{bm}}(\rho, t)$ , where  $\rho = \sqrt{y^2 + z^2}$  is the radial coordinate. The initial condition  $t = 0$  is assumed to correspond to the bone state at the onset of osteoporosis. A constant compressive force  $N(t) \equiv 0.4$  kN and constant bending moment around the  $z$  axis  $M_z(t) \equiv 2$  kN · m,  $M_y(t) \equiv 0$ , are assumed when calculating the stresses redistribution. Below, we first show how the bone volume fraction  $f_{\text{bm}}(\rho, t)$  evolves by means of Eq. (5) from a typically expected radial profile, and we determine the medullary cavity expansion that this evolution induces (Section 3.1). In a second numerical experiment, we calculate the “inverse problem”, i.e., we use morphological data by Feik et al. [2] compiled into an experimentally observed average medullary cavity expansion in men to determine what initial bone state would have generated this medullary expansion (Section 3.2).

### 3.1 Evolution of a typical bone volume fraction distribution

In Figure 2a, the bone volume fraction radial profile  $f_{\text{bm}}(\rho, t)$  is shown every 10 years from the onset of osteoporosis ( $t = 0$ ) for 50 years (until  $t = 50$ ). The assumed initial bone volume fraction profile at  $t = 0$  (solid line) is a sigmoid function of  $\rho$  with value zero for  $\rho \lesssim 3.3$  mm (medullary cavity), sharply increasing to 0.75 until  $\rho \approx 6.3$  mm (endocortical region) and more slowly increasing to 0.99 (intracortical region) until  $\rho = 12$  mm (periosteum, bone radius). Figure 2b and 2c show the corresponding changes in the radial profile of internal stresses  $\sigma(\rho, \theta, t)$  and specific surface  $s_V(\rho, t)$  across the midshaft. In contrast to  $f_{\text{bm}}$  and  $s_V$ , the internal stresses  $\sigma$  are not rotation-symmetric due to the assumed bending loading condition. The evolution of  $\sigma$  is shown at three angles  $\theta$  of the polar coordinate system, where  $\theta$  is measured from the  $y$  axis. The full polar distribution of stresses is shown in Figure 2e at  $t = 50$  years.

The bone volume fraction in Figure 2a is seen to decrease in all regions of the bone cross-section due to the simulated osteoporotic condition. However, as expected from Eq. (5), bone loss is more pronounced in the endocortical-to-intracortical region, where the specific surface is high. High bone volume fractions near the periosteum are comparatively more preserved. In the endocortical region, the bone volume fraction profile is both lowered and shifted towards the periosteum by the progression of osteoporosis, resulting in a more gradual increase of bone volume

fraction than the initial profile.

The radial profile of the specific surface (Figure 2c) gradually evolves such that its maximum originally at  $\rho \approx 5.5$  mm is shifted towards the periosteum. The position of this maximum corresponds to the intersection between the bone volume fraction and the constant value  $f_{\text{bm}}^* \approx 0.63$  in Figure 2a because  $f_{\text{bm}}^*$  maximises the function  $s_V(f_{\text{bm}})$  in Eq. (7). Taking  $f_{\text{bm}}^*$  as the threshold value to define the transition between medullary cavity and cortex, this shift of the maximum of the specific surface towards the periosteum corresponds to an expansion of the medullary cavity radius with age. This expansion is plotted separately in Figure 2d (thick solid line). Thin solid lines in Figure 2d correspond to the expansion of a medullary radius for other threshold values of  $f_{\text{bm}}$  as indicated by the labels. In this Figure, the onset of osteoporosis was assumed at 40 years of age. For the threshold value  $f_{\text{bm}}^*$ , the increase in medullary radius is initially slow, then accelerates at age  $\approx 55$ . The cortical wall thickness corresponds to the distance between bone radius (here assumed fixed at 12 mm) and medullary cavity radius, and is shown by the gray-shaded area. The expansion of the medullary cavity is therefore associated to a thinning of the cortical wall thickness.

These changes in morphological parameters are associated with a gradual transfer of the internal stresses towards the periosteum for  $\theta = 0$  and  $\theta = \pi/2$  (Figure 2b), whilst the stress radial profile at  $\theta = 0$  changes little. Interestingly, Figure 2b suggests that for each polar angle  $\theta$ , there is well-defined radius below which stresses are decreased and above which stresses are increased. The polar dependence of this radius can be appreciated in Figure 2f. In Figure 2f, isolines of the difference between initial stress distribution and stress distribution after 50 years of osteoporosis are shown. The above-mentioned  $\theta$ -dependent radius corresponds to the intersection between  $\sigma(\rho, \theta, t = 0)$  and  $\sigma(\rho, \theta, t = 50)$ , and so to the zero isoline in Figure 2f, shown as a thick gray line. The region where stresses are increased is shaded with blue tones and the region where stresses are decreased is shaded with yellow-red tones.

### 3.2 Determination of bone volume fraction near the endosteum from an observed medullary cavity expansion

As explained in Appendix B, it is possible to use the model to evolve the system backwards in time. This can be used to take as input a given medullary cavity expansion and deduce from it the distribution of

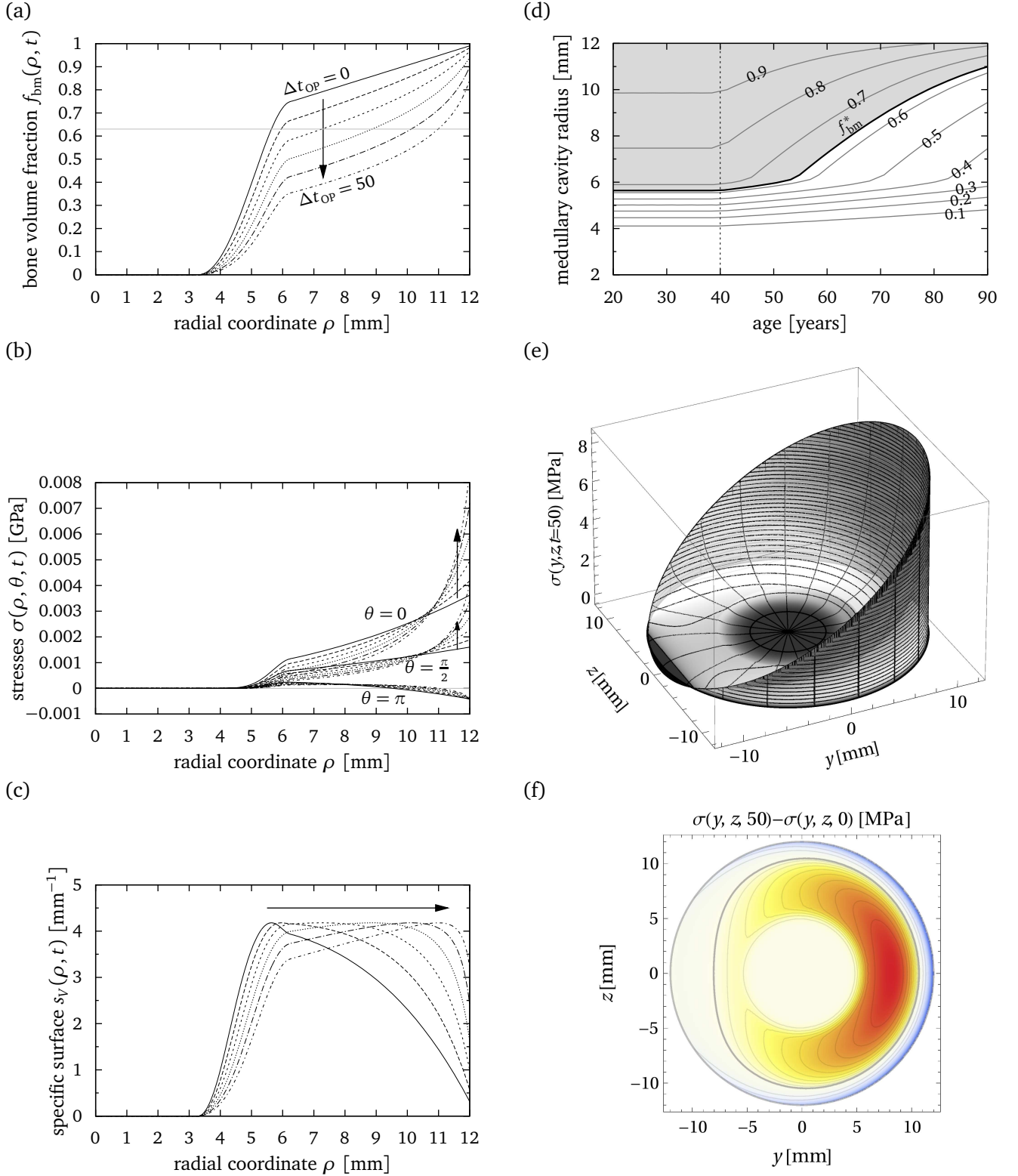


**Figure 2** – (a)–(c) Calculated radial profiles shown every 10 years since onset of osteoporosis for (a) bone volume fraction; (b) internal stresses at three different polar angles; (c) specific surface. The arrows indicate the evolution of the profiles with osteoporosis; (d) Calculated expansion of the medullary cavity radius. The effect of the threshold used to define the radius is shown. Thresholds from  $f_{bm} = 0.1$  to  $f_{bm} = 0.9$  are used (thin solid lines) in addition to the threshold  $f_{bm} = f_{bm}^*$  at which  $s_v$  is maximum (thick solid line). The filled region is indicative of the reduction in cortical wall thickness; (e) Stress distribution across the midshaft cross-section for compression and bending, exhibiting a neutral axis at  $y \approx -10$  mm; (f) Contour plot of the difference in internal stresses between initial bone state and bone state reached after 50 years of osteoporosis. Red tones: decrease in stresses; Blue tones: increase in stresses; Thick gray curve: no change in stresses (zero isoline).

bone volume fraction that leads to such an expansion. Mathematically, this “inverse problem” is only possible provided the medullary cavity radius is monotonously increasing. Also, the bone volume fraction profile can only be determined between the minimum and the maximum medullary cavity radii of the expansion. In Figure 3b, we show an experimental determination of medullary cavity expansion obtained by Feik et al. [2] from cross-sectional samples of the Melbourne Femur Collection. In the original data, samples were grouped in decade age categories (such as 31–40 years, 41–50 years etc.) and the medullary area was measured on each sample. Here we have transformed medullary area into medullary radius by assuming a rotation-symmetric medullary cavity and we have interpreted the value in a decade age category as the value at a single age in the timeline (e.g. 31–40 years  $\rightarrow$  30 years). Because the “inverse problem” requires a monotonously increasing radius, we took the data presented in [2, Fig. 5b] for males and discarded the first data point, as indicated by the hatched area in Figure 3b.

In Figure 3a, we show the bone volume fraction radial profile that reproduces the medullary cavity radius of Figure 3b when evolved from 30 years (solid line) to 90 years (double dashed line). As in Figure 2a, the calculated bone volume fraction profile is shown every 10 years and the medullary cavity radius is determined by the intersection of the profile with the constant value  $f_{bm}^*$  (dotted horizontal line). In Figure 3b, the minimum radius is  $\approx 6.4$  mm and the maximum radius is  $\approx 9.6$  mm, and so the bone volume fraction profile in Figure 3 is only determined between these radii as indicated by the excluded hatched areas.

## 4 Discussion

The study of age-related endocortical bone loss in humans is a challenging problem, with a multitude of possible causes, including biochemical, biomechanical and morphological regulations of bone remodelling. Whilst micro-CT imaging technology can give detailed insights into the bone microstructure at a given moment, to follow the evolution of bone microstructure with a degree of detail and a frequency that are sufficiently informative is (i) not currently possible without harmful radiation and (ii) would require several decades of study. Furthermore, soft tissues and bone cells are not seen in micro-CT bone scans. Two different approaches have been undertaken by biologists. Animals models of osteoporosis have been proposed, for which both micro-CT scans and histomorphometric analyses of bone samples can be performed,

providing both bone morphological parameters and biochemical information. However, particularly in small animals who lack secondary Haversian canals, the pathogenesis of osteoporosis is not the same as that in humans, whose loss of endocortical bone is believed to progress by expansion and coalescence of Haversian pores near the endosteum [5–7]. A second approach is to collect cross-sectional data from bone samples (either *ex vivo* or *post mortem*) and reconstruct pseudo time sequences by grouping the data by age categories [2, 3, 5–7]. The advantage of this approach is the direct measurement of human morphological properties of bone. The disadvantage is that often only a single point in time can be measured from an individual.

To our knowledge, there is currently no experimental work specifically studying the influence of the microscopic bone morphology on the development and/or activity of bone cells.<sup>6</sup> Such a morphological feedback on bone remodelling is challenging to investigate experimentally as it is not possible to “switch it off” to estimate its importance (in contrast to biochemical regulations that can be selectively inhibited by gene knock-outs in animal models), especially over the long time scales involved in osteoporosis. Computational modelling is a powerful tool that enables the testing of hypotheses for the underlying mechanisms responsible for age-related endocortical bone loss. Most importantly, computational modelling enables the extrapolation of data measured at a single point in time into a predicted evolution over several decades. This is of particular importance for the development of patient-specific assessment and treatment tools for osteoporosis.

The main result of this paper is the observation that a morphological feedback of the bone microstructure (specifically, of the bone specific surface) on the bone cells is able to explain (at least partly) the predominant loss of bone in the endocortical region. The nonuniformity of this loss can develop from a uniform baseline of bone imbalance per remodelling event as caused by systemic hormonal changes or overall changes in mechanical loading due to reduced physical activity. The loss of endocortical bone leads to an expansion of the medullary cavity that is compatible with experimentally observed rates. Furthermore, the deterioration of bone in the endocortical region leads

<sup>6</sup>Some effects of the curvature of the bone surface on osteoblast activation and/or osteoblast activity are known to occur. *In vivo*, the refilling rate of cortical BMUs depends on the current radius of the closing cavity as evidenced by double tetracycline labelling techniques [29–31]. In an *in-vitro* setup, the local curvature of the bone substrate was also shown to influence the rate of bone formation [32].



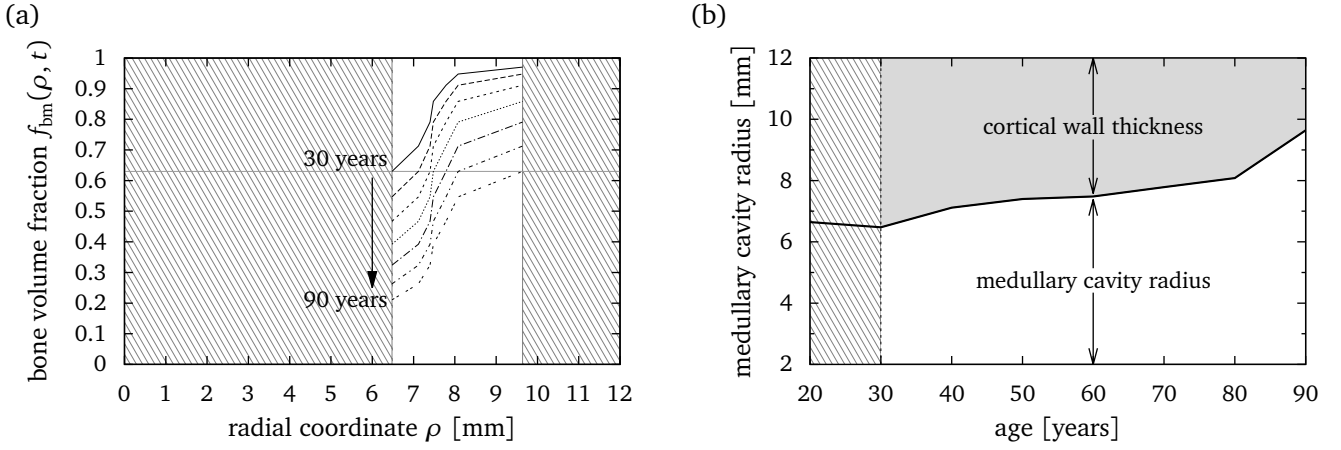


**Figure 3** – (a) Determination of bone volume fraction profiles in the encortical region (non-hatched area) from a given expansion of medullary cavity radius (b). The data in (b) is taken from male bone samples in Ref. [2, Fig. 5]. Only the monotonously increasing part of the curve (non-hatched area) can be used to determine the evolution of bone volume fraction profiles (see Appendix B).

to a transfer of the mechanical stresses towards the periosteum.

The evolution of the radial profile of bone volume fraction in the bone midshaft in Figure 2a is governed by a partial differential equation in time only. However, spatial nonuniformities enter the equation by means of the local availability of bone surface embodied by the specific surface  $s_V$ . Age-related cortical bone loss results in both an overall decrease in cortical bone volume fraction and a decrease in cortical wall thickness by loss on the endocortical surface. This is consistent with the experimental findings of Ref. [3].

The precise form of the expansion of the medullary cavity radius (Figure 2d) depends strongly on the assumed initial bone volume fraction profile and on the threshold value of bone volume fraction used to define the boundary between medullary cavity and cortex. The initial slow increase in medullary radius is due to the loss of bone in the region  $3.3 \text{ mm} \lesssim \rho \lesssim 6 \text{ mm}$  (endocortical region) in which bone volume fraction increases sharply with the radial coordinate  $\rho$  from 0 to 0.75. Once the sloped “plateau” of bone volume fraction for  $\rho \gtrsim 6 \text{ mm}$  (intracortical region) has reached the threshold bone volume fraction defining the medullary cavity boundary, the expansion of medullary radius increases rapidly before slowing down due to the relative preservation of bone volume fraction near the periosteum. In fact, choosing a different threshold volume fraction essentially delays or advances this general behaviour. From these results, one can deduce that for the influence of a morphological feedback, the sharper the transition between medullary cavity (zero bone volume fraction) and cortex, the slower the medullary cavity expansion. This observation emphasises the importance of building up “good bones” during growth, with high intracortical volume fractions [33].

We note that an acceleration of the medullary cavity expansion is seen in males in the 91–100 age category in [2, Fig. 5b] (Figure 3b). Whilst the calculation of the bone volume fraction leading to this experimental medullary expansion (Figure 3b) shows a similar sharp wall followed by a “sloped plateau” as in Figure 2a, other physiological factors not accounted for in our model may play a role in this experimentally observed acceleration of the medullary expansion, such as a difference in hormonal imbalance with advancing age that could lead to an increased bone imbalance per remodelling event.

Figures 2b and 2e clearly show that internal stresses become increasingly and disproportionately redistributed on the strongest part of the bone midshaft, i.e., towards the bone periphery. This disproportionate redistribution is likely to put the bone integrity at risk. Indeed, the periosteum is a surface with low remodelling rate [4, 34]. An acceleration of micro-crack generation at the periosteum can be expected, increasing the risk of a macroscopic fracture.

Increased stresses towards the periosteum may also account for a conservation of intracortical pore area. In the current model, a mechanical feedback to form bone at the periosteum and to slow down bone imbalance at endocortex is not explicitly taken into account.<sup>7</sup> Figure 2f suggests that a potential mechanical feedback based on internal stresses would lead to further nonuniformities in the evolution of the distribution of bone volume fraction in the midshaft. Indeed, the region in which stresses are increased and the region in which stresses are decreased by the simulated osteoporotic condition have an asymmetric boundary as shown by the thick gray line in Fig-

<sup>7</sup>In fact, setting the bone imbalance to  $-2\mu\text{m}/\text{year}$  in Eq. (6) could be assumed to implicitly account for a mechanical feedback at the endocortex.

ure 2f. The mechanical feedback would be particularly weak near the mechanical neutral axis induced by the bending loading condition and seen in Figure 2e near  $y \approx -10$  mm. Figure 2f also suggests that bone loss would be accelerated by a mechanical feedback in the endocortical region where stresses are higher, concurrently to an increased bone formation at the periosteum in this area, suggesting an outward shift of the cortex and so an evolving bone shape.

In this work, bone tissue was regarded as being solely composed of pores (vascular porosity) and mineralised bone matrix. In particular, osteoid deposited by active osteoblasts was assumed to become ‘instantly’ mineralised. Osteoporosis is an evolving bone disorder, that transitions from high turnover rate with low imbalance to mid-to-high turnover rate (possibly induced by secondary hyperparathyroidism) with a gradually increasing lack of formation [4, 9]. These differences in turnover rates modify the local volume fraction of osteoid. Increased turnover rate temporarily lowers the degree of mineralisation of bone and reduces the stiffness properties of bone [13, 17]. Here, only the morphological dimension of the progression of osteoporosis was considered. Changes in the degree of mineralisation of the bone matrix will be the subject of future works. We also note that osteoid asymmetrises the availability of bone surface between osteoblasts and osteoclasts. Indeed, active osteoclasts rarely resorb bone covered by osteoid, but active osteoblasts deposit osteoid on a previously laid osteoid layer.

In conclusion, we found that the microscopic availability of bone surface within the tissue, needed for resorption and formation processes to occur, is potentially a significant factor in focal bone loss predominantly occurring near the endocortical wall in osteoporosis. Furthermore, the gradual redistribution of the internal stresses towards the periosteum is suggestive of the possibility to induce modelling responses at the periosteum by mechanical feedback. Age-related endocortical bone loss involves a variety of biochemical and biomechanical processes that were not explicitly included in the model. Our model enables the extraction of the influence of the microscopic availability of bone surface. This influence is not easily assessed experimentally. Potential differences between experimental data on the evolution of bone volume fraction and the results of the model can therefore be attributed to these other influences, in particular a biomechanical feedback inducing other nonuniformities in the evolution of bone volume fraction.

## Acknowledgements

PP gratefully acknowledges financial support from the Australian Research Council (Project number DP0988427).

## Appendix A Semi-analytic implicit solution

The governing equation of the bone volume fraction has the form:

$$\frac{\partial}{\partial t} f_{\text{bm}}(\mathbf{r}, t) = -\eta s_V(f_{\text{bm}}(\mathbf{r}, t)). \quad (17)$$

with  $\eta = 2\mu\text{m}/\text{year}$ . This equation can be integrated in time at each location  $\mathbf{r}$ :

$$\int_0^t dt \frac{(\partial/\partial t) f_{\text{bm}}}{s_V(f_{\text{bm}})} = \int_{f_{\text{bm}}^0(\mathbf{r})}^{f_{\text{bm}}(\mathbf{r}, t)} \frac{df}{s_V(f)} = -\eta t. \quad (18)$$

Denoting by  $g(f)$  a primitive of  $1/s_V(f)$ , one can thus write the solution in the following implicit form:

$$g(f_{\text{bm}}(\mathbf{r}, t)) - g(f_{\text{bm}}(\mathbf{r}, 0)) = -\eta t. \quad (19)$$

When  $s_V(f)$  is a polynomial, one may use the representation:

$$\frac{1}{s_V(f)} = \sum_{i=1}^n \frac{A_i}{f - f_i}, \quad (20)$$

where  $A_i$  are (real) constants and  $f_i$  the (possibly complex) roots of  $s_V(f)$ , with  $f_1 = 0$  and  $f_2 = 1$ . Depending on the degree of the polynomial fit used for  $s_V(f)$ , these roots can be determined either numerically or analytically. For the particular fifth order polynomial proposed in Eq. (7) one has (with  $A_i$  in millimetre):

$$\begin{aligned} f_1 &= 0, & f_2 &= 1, & f_3 &\approx -0.611, \\ f_4 &\approx -0.55 - 0.7i, & f_5 &\approx 0.55 + 0.7i, \\ A_1 &\approx -2.04, & A_2 &\approx 0.89, & A_3 &\approx 0.55, \\ A_4 &\approx 0.30 - 0.63i, & A_5 &\approx 0.30 + 0.63i \end{aligned} \quad (21)$$

For polynomial  $s_V(f)$ , the function  $g(f)$  has thus the general form:

$$g(f) = \sum_{i=1}^n A_i \ln(f - f_i) = \ln \left( \prod_{i=1}^n (f - f_i)^{A_i} \right), \quad (22)$$

and the bone volume fraction  $f_{\text{bm}}(\mathbf{r}, t)$  can be determined by solving the implicit algebraic equation (using Eq. (22) in Eq. (19)):

$$\prod_{i=1}^n (f_{\text{bm}}(\mathbf{r}, t) - f_i)^{A_i} = \prod_{i=1}^n (f_{\text{bm}}(\mathbf{r}, 0) - f_i)^{A_i} e^{-\eta t} \quad (23)$$

This equation can also provide an implicit equation for the evolution of the medullary cavity. Assuming a cylindrical geometry, the medullary cavity radius  $\rho^*(t)$  at time  $t$  is defined by  $f_{\text{bm}}(\rho^*(t), t) = f^*$ , where  $f^*$  is the value of bone volume fraction chosen to define the endocortical wall, for example,  $f^* = 0.63$  at which the specific surface is maximum. From Eq. (23), one thus has:

$$\prod_{i=1}^n (f_{\text{bm}}(\rho^*(t), 0) - f_i)^{A_i} = \text{const } e^{\eta t} \quad (24)$$

## Appendix B Determination of the endocortical volume fraction profile at an earlier age

Reversing time in the governing equation for bone volume fraction (17) provides the evolution equation

$$\frac{\partial}{\partial \bar{t}} f_{\text{bm}}(\mathbf{r}, \bar{t}) = +\eta s_V(f_{\text{bm}}(\mathbf{r}, \bar{t})), \quad (25)$$

i.e., bone volume fraction increases with reversed time  $\bar{t} = -t$ . Because  $f_{\text{bm}}$  is the only state variable in the model presented here, one may determine the history of bone volume fraction from its current profile only. When other variables participate in determining the state of the system (such as bone cell densities in more comprehensive models of bone cell populations), this reversal is more complex and also numerically unstable.

In this appendix, we show that it is in fact sufficient to know the expansion of the medullary cavity in time to deduce the volume fraction profile at an earlier age (in particular, at the onset of osteoporosis) in the endocortical region. (This property has been used in Figure 3 with the evolution of the medullary cavity area estimated in Ref. [2, Fig. 5].) For simplicity, a rotation-symmetric cylindrical bone shaft is assumed. From Eq. (24), it is clear that if the medullary cavity radius  $\rho^*(t)$  is a monotonic increasing function of  $t \geq 0$  with values in the range  $[\rho_0, \rho_1]$ , one can solve Eq. (24) for  $f_{\text{bm}}(\rho, 0)$  for all  $\rho \in [\rho_0, \rho_1]$ . Indeed, it is sufficient to find the (unique) time  $\tilde{t}$  at which  $\rho^*(\tilde{t}) = \rho$  and to invert the implicit algebraic equation for  $f_{\text{bm}}(\rho, 0)$  obtained by setting  $t = \tilde{t}$  in Eq. (24).

Another approach is to evolve the system backwards in time during the time period  $\tilde{t}$  defined above, from the initial volume fraction  $f_{\text{bm}}^*$  defining the endocortical wall. Indeed, this backwards evolution directly provides the volume fraction  $f_{\text{bm}}(\rho, 0)$ . This approach is easier to implement numerically as it does not require the knowledge of the roots  $f_i$  of the phenomenological function  $s_V(f)$ .

## References

- [1] Compston J (2011) Age-related changes in bone remodelling and structure in men: Histomorphometric studies, *J Osteoporosis* **2011**:108324
- [2] Feik SA, Thomas CDL and Clement JG (1997). Age-related changes in cortical porosity of the midshaft of the human femur, *J Anat* **191**:407–416
- [3] Iwamoto J, Takeda T, Otani T, and Yabe Yutaka (1998). Age-related changes in cortical bone in women: Metacarpal bone mass measurement study *J Orthop Sci* **3**:90–94
- [4] Seeman E (2008) Modeling and remodeling: The cellular machinery responsible for the gain and loss of bone's material and structural strength. In Bilezikian JP, Raisz LG and Martin TJ, editors. *Principles of bone biology*. 3rd ed: Elsevier.
- [5] Bell KL, Loveridge N, Reeve J, Thomas CDL, Feik SA and Clement JG (2001). Super-osteons (remodeling clusters) in the cortex of the femoral shaft: Influence of age and gender, *Anat Rec* **264**:378–386
- [6] Thomas CDL, Feik SA and Clement JG (2005). Regional variation of intracortical porosity in the midshaft of the human femur: age and sex differences, *J Anat* **206**:115–125
- [7] Thomas CDL, Feik SA and Clement JG (2006). Increase in pore area, and not pore density, is the main determinant in the development of porosity in human cortical bone, *J Anat* **209**:219–230
- [8] Zebaze RMD Ghasem-Zadeh A, Bohte A, Iuliano-Burns S, Mirams M, Price RI, Mackie EJ, Seeman E (2010). Intracortical remodelling and porosity in the distal radius and post-mortem femurs of women: a cross-sectional study, *The Lancet* **375**:1729–1736
- [9] Manolagas SC (2000), Birth and death of bone cells: Basic regulatory mechanisms and implications for the pathogenesis and treatment of osteoporosis, *Endocr Rev* **21**:115–137
- [10] Feng X and McDonald JM (2011). Disorders of bone remodeling, *Ann Rev Pathol Mech Dis* **6**:121–145
- [11] Martin RB (1972) The effects of geometrical feedback in the development of osteoporosis, *J Biomech* **5**:447–455
- [12] Martin RB (1984) Porosity and specific surface of bone, *CRC Crit Rev Biomed Eng* **10**:179–222
- [13] Hellmich Ch, Ulm F-J and Dormieux L (2004) Can the diverse elastic properties of trabecular and cortical bone be attributed to only a

- few tissue-independent phase properties and their interactions?, *Biomech Model Mechanobiol.* **2**:219–238
- [14] Grimal Q, Raum K, Gerisch A and Laugier P (2011) A determination of the minimum sizes of representative volume elements for the prediction of cortical bone elastic properties. *Biomech Model Mechanobiol* **10**:925–937
- [15] Pivonka P, Zimak J, Smith DW, Gardiner BS, Dunstan CR, Sims NA, Martin TJ and Mundy GR (2008). Model structure and control of bone remodelling: A theoretical study, *Bone* **43**:249–263
- [16] Pivonka P, Buenzli PR, Dunstan CR (2012). A systems approach to understanding bone cell interactions in health and disease. In *Cell interactions*, Editor Gowder S. To appear. ISBN 980-953-307-341-0
- [17] Boivin G and Meunier PJ (2002). Changes in bone remodeling rate influence the degree of mineralization of bone, *Connect Tissue Res* **43**:535–537
- [18] Robling AG and Stout SD (1998) Morphology of the drifting osteon, *Cells Tissues Organs* **164**:192–204
- [19] Parfitt AM (1983). The physiological and clinical significance of bone histomorphometric data. In Recker RR (Ed.), *Bone histomorphometry: Techniques and interpretation*. CRC Press, Boca Raton, pp. 143–223.
- [20] Martin RB, Burr DB and Sharkey NA (1998). *Skeletal Tissue Mechanics* (New York: Springer)
- [21] Komarova SV, Smith RJ, Dixon SJ, Sims SM and Wahl LM (2003). Mathematical model predicts a critical role for osteoclast autocrine regulation in the control of bone remodeling *J. Theor. Biol.* **229**:293–309
- [22] Lemaire V, Tobin FL, Greller LD, Cho CR, Suva LJ (2004). Modeling the interactions between osteoblast and osteoclast activities in bone remodeling, *J Theor Biol* **29**:293–309
- [23] Pivonka P, Buenzli PR, Scheiner S, Hellmich Ch and Dunstan CR (2012) The influence of bone surface availability in bone remodelling—A mathematical model including coupled geometrical and biomechanical regulations of bone cells. Preprint: [arxiv:1201.3170](https://arxiv.org/abs/1201.3170)
- [24] Sankar BV (2001) An elasticity solution for functionally graded beams, *Comp Sci Technol* **61**:689–696
- [25] Yavari A, Sarkani S and Reddy JN (2001). On nonuniform Euler–Bernoulli and Timoshenko beams with jump discontinuities: application of distribution theory, *Int J Solids Struct* **38**:8389–8406
- [26] Alpdogan C (2008) Refined beam theories for inhomogeneous, anisotropic cylinders with arbitrary cross-sectional shape. PhD thesis, University of California, Los Angeles.
- [27] Landau LD, Lifshitz EM (1970) *Theory of elasticity* (Course of Theoretical Physics, **Vol. 7**), 2nd ed. (London: Pergamon Press)
- [28] van Oers RFM, Ruimerman R, Tanck E, Hilbers PAJ, Huiskes R (2008). A unified theory for osteonal and hemi-osteonal remodeling, *Bone* **42**:250–259.
- [29] Lee WR (1964) Appositional bone formation in canine bone: a quantitative microscopic study using tetracycline markers, *J Anat Lond* **98**:665–677
- [30] Manson JD and Waters NE (1965). Observations on the rate of maturation of the cat osteon, *J Anat Lond* **99**:539–549
- [31] Mertz LN, Martin RB and Turner AS (2003). Histomorphometric analysis of the effects of osteocyte density on osteonal morphology and remodeling, *Bone* **33**:753–759
- [32] Rumper M, Woesz A, Dunlop JWC, van Dongen JT and Fratzl P (2008), *J R Soc Interface* **5**:1173–1180.
- [33] Rizzoli R, Bianchi ML, Garabédian M, McKay HA, Moreno LA (2010) Maximizing bone mineral mass gain during growth for the prevention of fractures in the adolescents and the elderly, *Bone* **46**:294–305
- [34] Orwoll ES (2003) Toward an expanded understanding of the role of the periosteum in skeletal health, *J Bone Miner Res* **18**:949–954



This figure "fig-bone-beam-rve.png" is available in "png" format from:

<http://arxiv.org/ps/1206.6071v1>